2018

Restructuring Controllers to Accommodate Plant Nonlinearities

Kushal Sahare
University of Massachusetts Amherst

RESTRUCTURING CONTROLLERS TO ACCOMMODATE PLANT NONLINEARITIES

A Thesis Presented

by

KUSHAL SAHARE

Submitted to the Graduate School of the
University of Massachusetts Amherst in partial fulfillment
of the requirements for the degree of

MASTER OF SCIENCE IN MECHANICAL ENGINEERING

February 2018

Department of Mechanical and Industrial Engineering

RESTRUCTURING CONTROLLERS TO ACCOMMODATE PLANT NONLINEARITIES

A Thesis Presented

by

KUSHAL SAHARE

Approved as to style and content by:

Kourosh Danai, Chair

Mathew Lackner, Member

Frank Sup, Member

Sundar Krishnamurty, Department Head
Department of Mechanical and Industrial Engineering

This thesis is dedicated to my parents

ACKNOWLEDGMENTS

First and foremost I offer my sincerest gratitude to my supervisor, Dr Kourosh Danai, who has supported me throughout my thesis with his patience and knowledge. I attribute the level of my Masters degree to his encouragement and effort and without him this thesis would not have been completed or written. One simply could not wish for a better or friendlier supervisor. I would also like to thank Dr William La Cava. This thesis is entirely built on the algorithm developed by him. I would like to thank my committee members Professor Mathew Lackner and Professor Frank Sup for their interest in my work.

Finally, I would like to acknowledge friends and family who supported me during my time here. First and foremost I would like to my parents and siblings for their constant love and support. Kiran Iyer, Ashok Obuli, Ravi Agrawal and Vijeta Deshpande made my time here at UMASS a lot more fun.

ABSTRACT

RESTRUCTURING CONTROLLERS TO ACCOMMODATE PLANT NONLINEARITIES

FEBRUARY 2018

KUSHAL SAHARE

B.Tech., INDIAN INSTITUTE OF TECHNOLOGY GUWAHATI

M.S.M.E., UNIVERSITY OF MASSACHUSETTS AMHERST

Directed by: Professor Kourosh Danai

This thesis[1] explores the possibility of controller restructuring for improved closed-loop performance of nonlinear plants using a gradient based method of symbolic adaptation- *Model Structure Adaptation Method (MSAM)*. The adaptation method starts with a controller which is a linear controller designed according to the linearized model of the nonlinear plant. This controller is then restructured into a series of nonlinear candidate controllers and adapted iteratively toward a desired closed-loop response. The noted feature of the adaptation method is its ability to quantify structural perturbations to the controllers. This quantification is important in scaling the structural Jacobian that is used in gradient-based adaptation of the candidate controllers. To investigate this, two nonlinear plants with unknown nonlinearities viz., nonlinear valve and nonlinear inverted pendulum are chosen. Furthermore, the properties of restructured controllers obtained for two systems, stability, effect of measurement noise, reachability, scalability and algorithmic issues of MSAM are studied and compared with the starting controller.

[1]The work in this thesis formed the basis of a journal publication [1]

TABLE OF CONTENTS

LIST OF TABLES

LIST OF FIGURES

Figure **Page**

CHAPTER 1

INTRODUCTION

When the agility of feedback can compensate for mild plant nonlinearities, linear controllers designed according to the linearized model of the plant will suffice [4]; and in cases when the plant nonlinearities are too severe for a single linear controller across the range of operating points, gain scheduling can be employed to incorporate different linear controllers at different operating points [2]. The leap to nonlinear control can be made, for improved performance, when accurate models of plant nonlinearities exist to allow nonlinear controller design [5, 6, 7]. This thesis offers an alternative method of empirical controller development wherein a starting, generally linear, controller is expanded into a nonlinear controller with coupled components to attain improved closed-loop performance.

The most common platform for empirical development of nonlinear controllers has been neural networks [8, 9]. However, these controllers have a "black box" form precluding analysis that requires the transparency of form/structure. In an attempt to attain transparency, one can use symbolic regression wherein the process variables, inputs, and parameters (constants) are treated as symbols and integrated as blocks to form candidate models. Free of restrictions on the form (structure) of candidate controllers, the search can be conducted by genetic programming (GP) for controllers generating best-fit closed-loop outputs to the desired response [10]. However, symbolic regression is computationally expensive, requiring anywhere from thousands to billions of evaluations. While so many evaluations can be accommodated in open-loop by algebraic manipulation of the time

series representing measured observations and their derivatives, they are infeasible in closed-loop wherein the system response needs to be obtained via simulation for each adopted controller. As such, the use of evolutionary and/or genetic algorithms in controls has been confined to parameter optimization [11, 12] or search among a limited number of structural components [13].

Whereas the method proposed in this thesis also restricts the search space to a limited number of candidate controllers, it formulates them by restructuring an initial controller instead of relying on pre-formulated fixed structures. Furthermore, it incorporates pliability in these restructured controllers by inclusion of exponents that can be adapted toward their suitable form. The adaptation of these exponents, which amounts to a local search around the initial controller, is performed by the Model Structure Adaptation Method (MSAM) [14]. A key feature of MSAM, that enables the implementation of gradient-based adaptation as its search mechanism, is its quantification of structural changes to the controllers. MSAM uses this metric to scale the structural sensitivities such that they will remain robust to parametric error during adaptation. The proposed controller restructuring is schematized in Fig. 1.1, which resembles the strategy used in iterative feedback tuning (IFT) [15, 16, 17, 18]. In this scheme, G represents the nonlinear plant and G_c the controller. Whereas in IFT the parameters of G_c are adjusted/tuned, in MSAM a candidate set of controller formats with pliable structures are considered which are adapted iteratively to produce the desired response y^d to the reference input r. Therefore, MSAM differs from iterative tuning in that it changes the controller structure instead of just its parameters toward the desired response. In Fig. 1.1, u denotes the control effort, n the measurement noise, and $\tilde{y}$ represents the error between the closed-loop response of the system $\hat{y}$ and its desired response y^d.

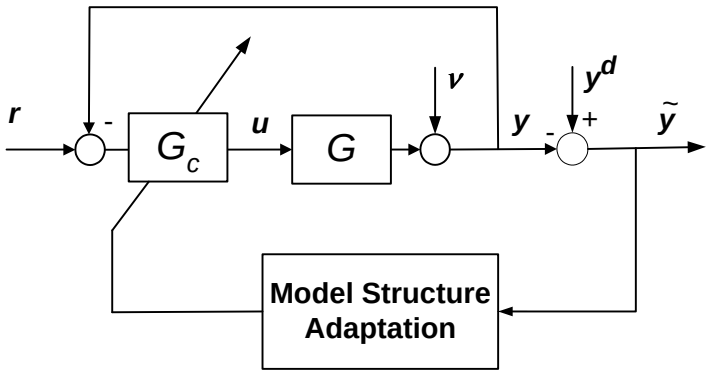

Figure 1.1. Contoller adaptation by MSAM

CHAPTER 2

THE MODEL STRUCTURE ADAPTATION METHOD (MSAM)

2.1 Introduction

Model structure adaptation method is a gradient-based method of symbolic adaptation for continuous dynamic models [14, 19]. This method starts with an initial model (e.g., derived from first-principles) and amends its components in symbolic form. The salient feature of this method is its use of a metric for symbolic changes to the model. This metric, which is essential for defining the structural sensitivity of the model, not only accommodates algebraic evaluation of candidate models in lieu of less reliable simulation-based evaluation but also makes possible the implementation of gradient-based optimization in symbolic adaptation.

2.2 Formulation

In MSAM, the initial controller $u = \mathbf{M}_{\boldsymbol{\Theta}}$ is considered to be the weighted sum of individual components M_i, as

$$\mathbf{M}_{\boldsymbol{\Theta}} = \sum_{i=1}^{Q} \theta_i M_i = \boldsymbol{\Theta}^T \mathbf{M} \tag{2.1}$$

where $\mathbf{M} = [M_1, \ldots, M_Q]^T$ comprises components M_i that are products of combinations of state variables x_i included in the state vector $\mathbf{x} = [x_1, \ldots, x_n]^T$. For instance, in context of a PID controller, the initial controller is

$$\mathbf{M}_{\widetilde{\boldsymbol{\Theta}}} = K_p \epsilon(t) + K_i \int \epsilon(t) \mathrm{d}t + K_d \mathrm{d}\epsilon/\mathrm{d}t \tag{2.2}$$

where $\epsilon(t) = r(t) - \hat{y}(t)$; $\mathbf{M} = [M_1\ M_2\ M_3]^T = [\epsilon(t),\ \int \epsilon(t)\mathrm{d}t,\ \mathrm{d}\epsilon/\mathrm{d}t]^T$ with the corresponding parameter values $\mathbf{\Theta} = [\theta_1\ \theta_2\ \theta_3]^T = [K_p,\ K_i,\ K_d]^T$. The fidelity of the controller can be evaluated by how closely the closed-loop response of the nonlinear plant matches the desired response y^d, as represented by their difference $\tilde{y}_{\widehat{\mathbf{M}}}$ where $\widehat{\mathbf{M}}$ denotes the candidate controller. The fitness function in MSAM is often defined as

$$F = \frac{\rho(\hat{y}, y^d)}{\sum_{k=1}^{N} |\tilde{y}(t_k)|} \tag{2.3}$$

where $\rho(\hat{y}, y^d)$ denotes the correlation coefficient between the closed-loop response $\hat{y}$ and the desired response y^d, computed as

$$\rho(\hat{y}, y^d) = \frac{C_{\hat{y}y^d}}{\sigma_{\hat{y}}\sigma_{y^d}} \tag{2.4}$$

where $C_{\hat{y}y^d}$ is the covariance of $\hat{y}$ and y^d, and $\sigma_{\cdot}$ denotes standard deviation. The larger the fitness value, the closer the closed-loop response is to its target, therefore, this fitness function is used primarily to evaluate the fitness of various candidate controllers in the first stage of adaptation by MSAM. It should be noted here that $\hat{y}$ is not only a function of the controller structure $\widehat{\mathbf{M}}$ and its parameters $\mathbf{\Theta}$ but also the reference r, the plant G, and noise n. Given that $\tilde{y}$, in addition to its role in the fitness function, is the basis for adaptation of the candidate controller $\widehat{\mathbf{M}}$, it is imperative to have persistence of excitation [8] by $\tilde{y}(t)$.

With the commonality of r, G, and y^d among the candidate controllers, the output error $\tilde{y}$ is a function of the candidate controller $\widehat{\mathbf{M}}$ and its parameters $\mathbf{\Theta}$. If one assumes that an ideal controller $\mathbf{M}^*$ with the ideal parameters $\mathbf{\Theta}^*$ exists that could generate the desired response y^d, then the output error $\tilde{y}$ is mainly caused by the structural mismatch; i.e., $\widetilde{\mathbf{M}} \neq \mathbf{M}^*$ as well as the parametric error $\widetilde{\Delta\mathbf{\Theta}} = \mathbf{\Theta}^* - \widetilde{\mathbf{\Theta}}$. In IFT [15, 20], the controller form is assumed correct and the model parameters are tuned to reduce $\tilde{y}$. However, when the controller form is incorrect (i.e., $\widetilde{\mathbf{M}} \neq \mathbf{M}^*$),

parameter tuning will be superficial. Since structural accuracy of the controller transcends its parametric accuracy, MSAM focuses on structural adaptation of G_c.

Controller restructuring in MSAM is performed by adjusting each nominal component of the initial controller $\widetilde{M}_i$ as $\widetilde{M}_i \Longrightarrow \widetilde{M}_i \hat{f}_i(\mathbf{x})^{\gamma_i}$ to yield candidate controllers of the form

$$\widehat{\mathbf{M}}_{\widetilde{\mathbf{\Theta}}} \;=\; \sum_{i=1}^{Q} \tilde{\theta}_i \widetilde{M}_i \hat{f}_i(\mathbf{x})^{\gamma_i} = \widetilde{\mathbf{\Theta}}^T \widehat{\mathbf{M}} \tag{2.5}$$

where $\widehat{\mathbf{M}} = \left[\widetilde{M}_1 \hat{f}_1(\mathbf{x})^{\gamma_1},\ \ldots,\ \widetilde{M}_Q \hat{f}_Q(\mathbf{x})^{\gamma_Q}\right]^T$, the $\hat{f}_i$ are functions of individual state variables, such as $|x_i|$, $sign(x_i)$, $cos(x_i)$, etc., considered to improve the controller form, and the $\gamma_i \in \Re$ are exponents to achieve two goals:

(i) to mitigate the discrete nature of the introduced model change, and

(ii) to provide a mechanism for calibrating the degree of change to individual model components for higher granularity.

For instance, to restructure a PID controller into the nonlinear form

$$K_p \epsilon(t) \left|\mathrm{d}\epsilon/\mathrm{d}t\right|^{\gamma} + K_i \int \epsilon(t)\mathrm{d}t + K_d \mathrm{d}\epsilon/\mathrm{d}t \tag{2.6}$$

, the first component $\widetilde{M}_1 = \epsilon(t)$ needs to be changed to $\widehat{M}_1 = \epsilon(t) \left|\mathrm{d}\epsilon/\mathrm{d}t\right|^{\gamma}$. Assuming that the ideal controller structure $\mathbf{M}^*$ can be reached by the introduction of adjustments $\hat{f}$ to the initial controller structure $\widetilde{\mathbf{M}}$, the ideal controller will have the form

$$\mathbf{M}^* = \left[\widetilde{M}_1 f_1^*(\mathbf{x})^{\gamma_1^*},\ \ldots,\ \widetilde{M}_Q f_Q^*(\mathbf{x})^{\gamma_Q^*}\right]^T \tag{2.7}$$

Hence, the adaptation strategy entails applying adjustments of the form (2.5) to individual components of the initial controller $\widetilde{\mathbf{M}}$ during a round robin stage,

and then adapting the exponents γ_i to fine-tune the controller structure. The goal of MSAM is to mainly find the form

$$\mathbf{f}^* = \left[f_1^*(\mathbf{x}), \ldots, f_Q^*(\mathbf{x})\right]^T \tag{2.8}$$

in the first stage of adaptation, called round robin, and then fine-tune the exponents γ_i, to achieve $\mathbf{\Gamma} = [\gamma_1, \ldots, \gamma_Q]^T \implies \mathbf{\Gamma}^* = \left[\gamma_1^*, \ldots, \gamma_Q^*\right]^T$. For illustration purposes, selection of the best candidate controller in the first stage, followed by its adaptation in the second stage, is shown in Fig. 2.1. The plots in the first stage represent the fitness values of the candidate controllers during the first 15 iterations of adaptation. The under performing controllers are discarded for the second stage where adaptation is continued toward fine-tuning the exponents of the best-fit controller.

For gradient-based search in the round robin stage, the output error $\tilde{y}(t)$ is defined by its first-order approximation at the nominal parameter values $\tilde{\theta}_i$, and exponents $\widehat{\gamma}_i$, as

$$\tilde{y}_{\widehat{\mathbf{M}}}(t) = y^d(t) - \hat{y}_{\widehat{\mathbf{M}}}(t) - \tilde{y}_\theta \approx \sum_{i=1}^{Q} \widehat{\Delta\gamma}_i \left(\frac{\partial \hat{y}_{\widehat{\mathbf{M}}}(t)}{\partial \gamma_i}\right) = \tilde{y}_\gamma = \mathbf{\Phi}_\gamma \widehat{\Delta\mathbf{\Gamma}} \tag{2.9}$$

where $\tilde{y}_\theta = \sum_{i=1}^{Q} \widetilde{\Delta\theta}_i \left(\frac{\partial \hat{y}_{\widehat{\mathbf{M}}}(t)}{\partial \theta_i}\right)$ denotes the parametric error. Since potential collinearity between θ_i, γ_i pairs often hinders their concurrent adaptation, only the exponents are adapted iteratively for their larger influence on the error (in the absence of bifurcation) [14, 19]. Here, a key contribution of MSAM [14] is its introduction of the 'model perturbation magnitude' δM_i to quantify model changes affected by perturbations to the exponents γ_i in Eq. (2.5), as

$$\delta M_i = \frac{\sum_{k=1}^{N} \left|\left| \frac{\partial \hat{y}(t_k, \widehat{\mathbf{\Gamma}} + \delta\gamma_i, \widetilde{\mathbf{\Theta}})}{\partial \mathbf{\Theta}} - \frac{\partial \hat{y}(t_k, \widehat{\mathbf{\Gamma}}, \widetilde{\mathbf{\Theta}})}{\partial \mathbf{\Theta}} \right|\right|_2}{\sum_{k=1}^{N} \left|\left| \frac{\partial \hat{y}(t_k, \widehat{\mathbf{\Gamma}}, \widetilde{\mathbf{\Theta}})}{\partial \mathbf{\Theta}} \right|\right|_2} \tag{2.10}$$

to be used in the scaling of structural sensitivity, as

$$\partial\hat{y}(t,\widehat{\mathbf{\Gamma}},\widetilde{\mathbf{\Theta}})/\partial\gamma_i \approx \left(\hat{y}(t,\widehat{\mathbf{\Gamma}}+\delta\gamma_i,\widetilde{\mathbf{\Theta}}) - \hat{y}(t,\widehat{\mathbf{\Gamma}},\widetilde{\mathbf{\Theta}})\right)/\delta M_i \tag{2.11}$$

in lieu of $\delta\gamma_i$ in the denominator of the finite difference approximation of the output sensitivity.

The availability of the Jacobian $\mathbf{\Phi}_\gamma$ enables estimation of the exponential errors $\Delta\gamma_i$ according to nonlinear least-squares, as

$$\widehat{\Delta\mathbf{\Gamma}} = [\widehat{\Delta\gamma}_1,\ldots,\widehat{\Delta\gamma}_Q]^T = (\mathbf{\Phi}_\gamma^T\mathbf{\Phi}_\gamma)^{-1}\mathbf{\Phi}_\gamma^T\tilde{y}^N \tag{2.12}$$

and consequent adaptation of the exponents, as

$$\gamma_i(q+1) = \gamma_i(q) + \mu(q)\Delta\gamma_i(q) \tag{2.13}$$

where $\tilde{y}^N$ is the vector of sampled output error, q is the iteration number and $\mu(q)$ is the adaptation step size, determined at each iteration.

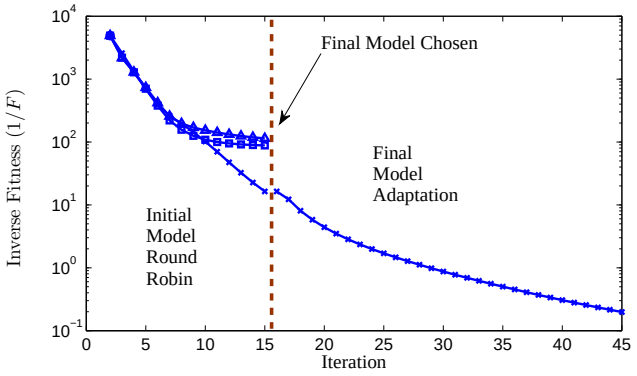

Figure 2.1. Illustration of candidate model selection by MSAM in the round robin stage, followed by further adaptation of the selected model in the second stage, as represented by the inverse of the fitness value for each model

CHAPTER 3

STUDY PLATFORMS

3.1 Study Platforms

Two closed-loop platforms are considered for studying the feasibility of MSAM. The first platform, as shown in [2], consists of a linear plant that is actuated by a nonlinear valve, representing a compartmentalized plant nonlinearity. Åström and Wittnemark [2] capitalize on knowledge of the actuator nonlinearity to cascade the linear (proportional plus integral (PI)) controller with the inverse function of the actuator model, so as to compensate for its nonlinearity. The PI controller was restructured by MSAM to replace the controller and cascaded inverse function. The second platform is the benchmark control of an inverted pendulum on a cart which presents an inherently nonlinear and unstable plant commonly controlled within small deviations from the vertical position. These two platforms are used to study the characteristics of the restructured controllers.

3.1.1 Nonlinear Actuator

The first platform, adopted from [2], is shown in Fig. 3.1 where the plant consists of a nonlinear actuator, proceeded by a linear process. The customized controller discussed in [2] is a PI controller with the parameters $K_p = 0.1$ and $T_i = 0.1$ cascaded with a nonlinear function that approximates the inverse of the actuator model. The nonlinear actuator model, the transfer function of the process, and the inverse actuator model used in [2] are shown in Table 3.1.

As discussed in [2], and shown in Fig. 3.2, the above closed-loop system generates different responses at different reference values, representing the limitation

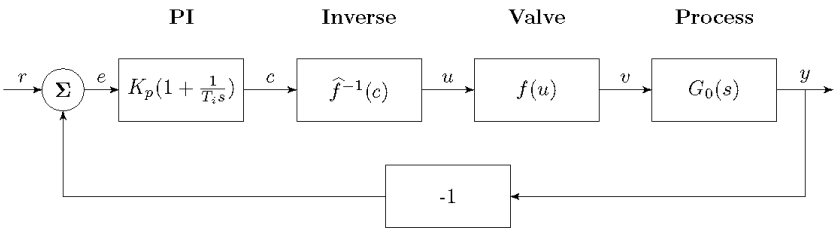

Figure 3.1. Block diagram of the first platform, consisting of a linear plant actuated by a nonlinear valve (Courtesy of Åström and Wittnemark [2])

of the inverse approximation $\widehat{f}^{-1}$ in neutralizing the actuator nonlinearity $f(u)$ at different reference values. A drawback of this solution is rooted in the deviation of $f(\widehat{f}^{-1}(c))$ from the ideal value of 1 at different reference values, except at $r = 1$ where the inverse function is exact and the response obtained is desired. Another drawback of this solution is its dependence on the accuracy of the modeled nonlinearity. To evaluate the significance of this dependence, the closed-loop step responses of the system at different reference values are compared in Fig. 3.3 with the step responses of two other systems representing slightly different actuator nonlinearities: $f(u) = u^{3.5}$ and $f(u) = u^{4.5}$. The results clearly indicate the considerable influence of misrepresented nonlinearity on the responses of the customized solution, particularly at higher reference values.

Table 3.1. Models of the individual blocks [2] in Fig. 3.1

Nonlinear Actuator	$v = f(u) = u^4$
Process	$G_0(s) = \frac{1}{(s+1)^3}$
Inverse Model	$f^{-1}(c) = \begin{cases} 0.433c & \text{if } 0 \leq \text{c} < 3 \\ 0.0538c + 1.139 & \text{if } 3 \leq \text{c} \leq 16 \end{cases}$

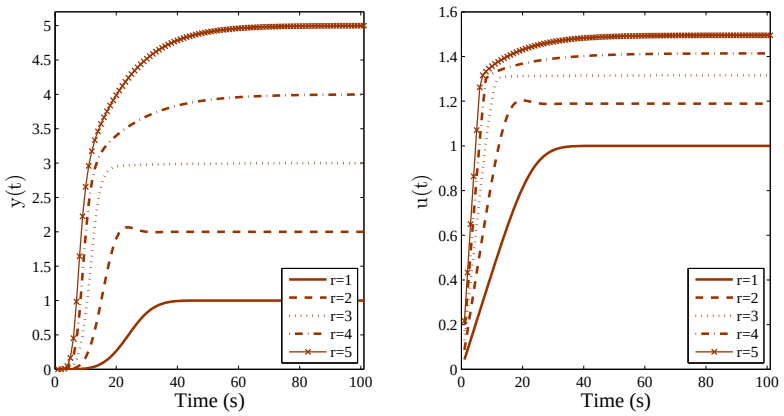

Figure 3.2. Step responses and control efforts of the closed-loop customized solution in Fig. 3.1 at different reference magnitudes

3.1.2 Inverted Pendulum on a Cart

The second platform, obtained from [3], is the classical inverted pendulum on a cart, as shown in Fig. 3.4 and modeled in Table 3.2. In this model, $x(t)$ denotes the position of the cart in the x direction, $\theta(t)$ denotes the angle of the pendulum from vertical, and $u(t)$ is the force applied to the cart. This model was simulated with the cart mass m' = 0.9 kg, the pendulum mass at the end of the massless rod represented as m = 0.1 kg, and the pendulum length represented as l = 0.235 m.

Table 3.2. Model of the inverted pendulum on a cart from [3]

$$\begin{aligned} \ddot{x} &= \frac{u+ml(\sin(\theta))\dot{\theta}^2-mg\cos(\theta)\sin(\theta)}{m'+m-m\cos^2(\theta)} \\ \ddot{\theta} &= \frac{u\cos(\theta)-(m'+m)g\sin(\theta)+ml(\cos(\theta)\sin(\theta))\dot{\theta}}{ml\cos^2(\theta)-(m'+m)l} \end{aligned}$$

The feature of interest to our study in this platform is the effectiveness of restructured controller in coping with plant nonlinearity beyond angles regulated by the linear controller. At small θ values, like those caused by low magnitude impulses to the pendulum, a linear controller, by state feedback, for example, can

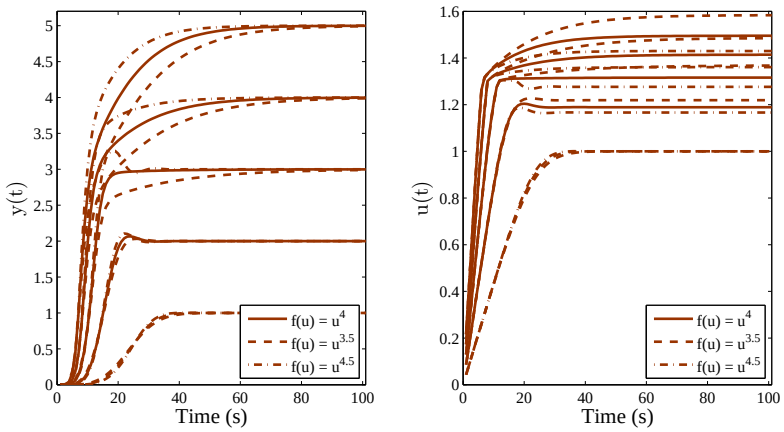

Figure 3.3. Effect of modeling inaccuracy on the step responses and control efforts of the closed-loop solution in Fig. 3.1

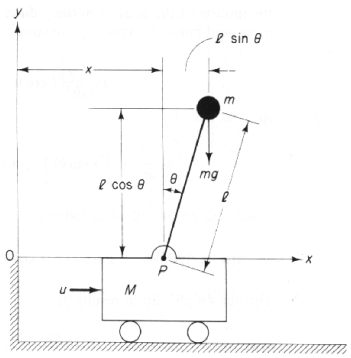

Figure 3.4. Inverted Pendulum on a cart used as the plant in the second study platform

maintain the upward position of the pendulum. But the nonlinearity at larger θ values will disturb the performance of linear control. This point is shown for a linear state-feedback controller of the form

$$u(t) = -K_1 x - K_2 \dot{x} - K_3 \theta - K_4 \dot{\theta} \tag{3.1}$$

with the gains $[K_1, K_2, K_3, K_4] = [-2.00, -3.84, 33.84, 7.22]$ locating the closed-loop poles at $s_{1,2,3,4} = -1, -2, -4.73, -4.73$ according to the linearized model of the pendulum. The closed-loop impulse responses of the pendulum to different impulse

magnitudes applied to the pendulum using this controller are shown in Fig. 3.5. It clearly indicates the effect of nonlinearity on the performance of the linear controller at higher impulse magnitudes.

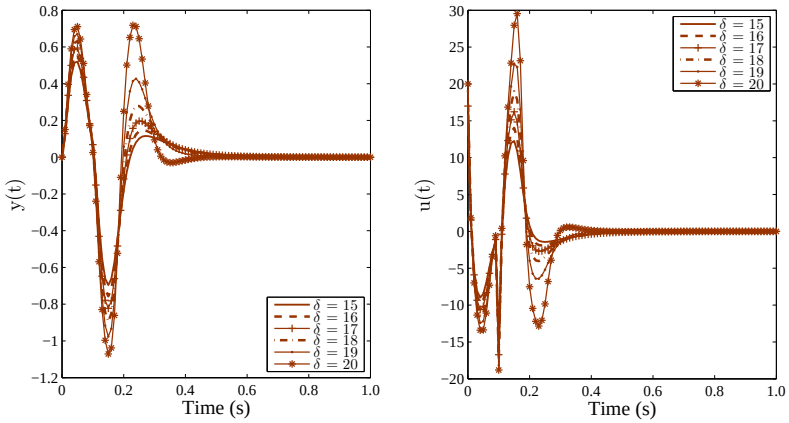

Figure 3.5. Closed-loop impulse responses ($y = \theta$) and control efforts of the inverted pendulum on a cart controlled by linear state feedback. Impulse magnitudes are in newton.

CHAPTER 4

RESTRUCTURED CONTROLLER

4.1 Restructured Controller

Controllers were restructured by MSAM for the two platforms according to the configuration in Fig. 1.1. The desired response y^d used for the nonlinear actuator was the step response of a standard second order model, the one for the inverted pendulum on a cart was the impulse response of the linear controller to the lowest magnitude impulse ($\delta = 15$ N) applied to the pendulum. The coupling functions $\hat{f}_i$ in Eq. (2.5) were the absolute values of the state variables, to avoid imaginary numbers due to exponentiation of negative numbers. The restructured controllers obtained for the above platforms are discussed separately.

4.1.1 Controller for the Nonlinear Actuator

A feature of restructured controllers is their case-specificity, which is rooted in the search mechanism for the exponents γ_i in Eq. (2.5). As in any gradient-based search, the robustness of the solution and its form not only depend on the convexity of the error surface presented during training, but also the search mechanism (NLS, in this case). As such, the choice of the desired response y^d plays a central role in the formulation of the solution. It is observed, for instance, that the more distant is the target from the initial closed-loop response, the better chance there is of finding a radically restructured controller. For case-specificity of restructured controllers, consider the controllers obtained at different reference magnitudes for the nonlinear actuator in Table 4.1. Here we arbitrarily used the step response of a

standard second order model ($\zeta = 1$, $\omega_n = 0.17$) as the desired response and the PI controller: $K_p\epsilon(t) + K_i \int \epsilon(t)\mathrm{d}t$ as the initial controller amended with the functions $[f_1, f_2] = [|\epsilon|, |\int \epsilon \mathrm{d}t|]$ in Eq. (2.5) for its restructuring. Each candidate controller was adapted for 15 iterations in the round robin phase and the best controller was further adapted for 20 more iterations in the final phase. Although the forms of the restructured controllers in Table 4.1 are the same for reference magnitudes of 1, 2, and 4, in one form, and for reference magnitudes of 3 and 5, in another form, they are not uniform across all reference magnitudes.

Table 4.1. Restructured controllers obtained at different reference values for the nonlinear actuator

Reference Value	Restructured Controller
1	$K_p\epsilon \left(\lvert\int \epsilon \mathrm{d}t\rvert\right)^{0.27} + K_i sgn(\int \epsilon \mathrm{d}t) \left(\lvert\int \epsilon \mathrm{d}t\rvert\right)^{0.80}$
2	$K_p\epsilon \left(\lvert\int \epsilon \mathrm{d}t\rvert\right)^{0.19} + K_i sgn(\int \epsilon \mathrm{d}t) \left(\lvert\int \epsilon \mathrm{d}t\rvert\right)^{0.82}$
3	$K_p sgn(\epsilon) \lvert\epsilon\rvert^{1.15} + K_i sgn(\int \epsilon \mathrm{d}t) \left(\lvert\int \epsilon \mathrm{d}t\rvert\right)^{0.81}$
4	$K_p\epsilon \left(\lvert\int \epsilon \mathrm{d}t\rvert\right)^{0.15} + K_i sgn(\int \epsilon \mathrm{d}t) \left(\lvert\int \epsilon \mathrm{d}t\rvert\right)^{0.78}$
5	$K_p sgn(\epsilon) \lvert\epsilon\rvert^{1.08} + K_i sgn(\int \epsilon \mathrm{d}t) \left(\lvert\int \epsilon \mathrm{d}t\rvert\right)^{0.78}$

To ameliorate their uniformity, restructuring of the controller for the first platform was performed with a staircase reference profile that included three reference magnitudes(viz., 1, 3, & 5), as shown in Fig. 4.1. Controller restructuring resulted in

$$u(t) = K_p\epsilon + K_i \left(\int \epsilon \mathrm{d}t\right) \quad \Longrightarrow$$
$$u(t) = K_p\epsilon(t) \left(\lvert\int \epsilon(t)\mathrm{d}t\rvert\right)^{0.04} + K_i sgn(\int \epsilon(t)\mathrm{d}t) \left(\lvert\int \epsilon(t)\mathrm{d}t\rvert\right)^{0.80} \tag{4.1}$$

with its response named "restructured" in Fig. 4.1. The response of the restructured controller is compared in Fig. 4.2 with those of the initial (PI) and customized (PI controller cascaded with the inverse model of the actuator) controllers. The results indicate more consistent rise times of the initial and restructured controllers

than the customized controller. They also indicate the far smaller overshoot of the restructured controller than the initial controller's, as the result of restructuring toward the desired response.

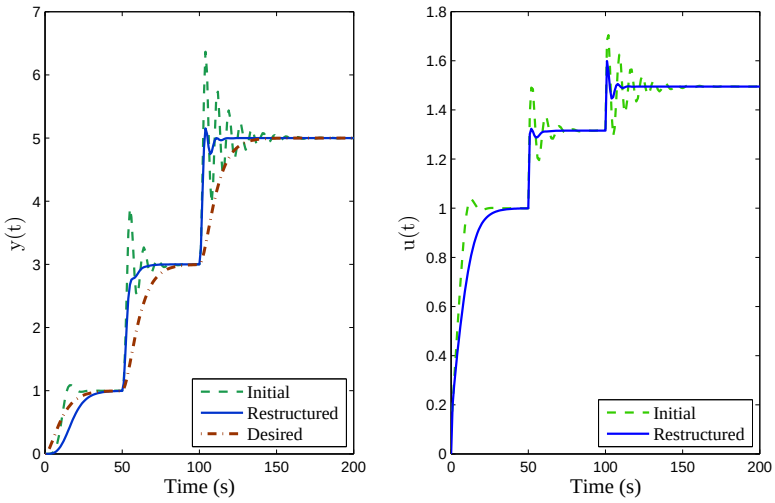

Figure 4.1. Step responses and control efforts of the restructured and initial (PI) controllers from the first platform shown with the desired response used for controller restructuring

As discussed earlier, an important feature of MSAM is the use of δM_i in Eq. (2.10) for scaling the columns of $\mathbf{\Phi}_\gamma$ in Eq. (2.11). A direct ramification of this scaling is ought to be the better quality of $\mathbf{\Phi}_\gamma$, that results in improved estimates of $\widehat{\Delta\mathbf{\Gamma}}$ when used in Eq. (2.12). The quality of $\mathbf{\Phi}_\gamma$ is illustrated by the range of condition numbers ($\lambda_{max}/\lambda_{min}$) of $\mathbf{\Phi}_\gamma$ in Table 4.2, computed with and without scaling by δM_i at different reference magnitudes with the nonlinear actuator. Since the closer is the condition number to unity the more separate (less collinear) are the columns of the matrix [21], the smaller condition numbers in Table 4.2 for $\mathbf{\Phi}_\gamma$ when scaled by δM_i should result in improved restructured controllers. This is verified by the smaller lowest absolute output error sums in Table 4.2 obtained during adaptation by scal-

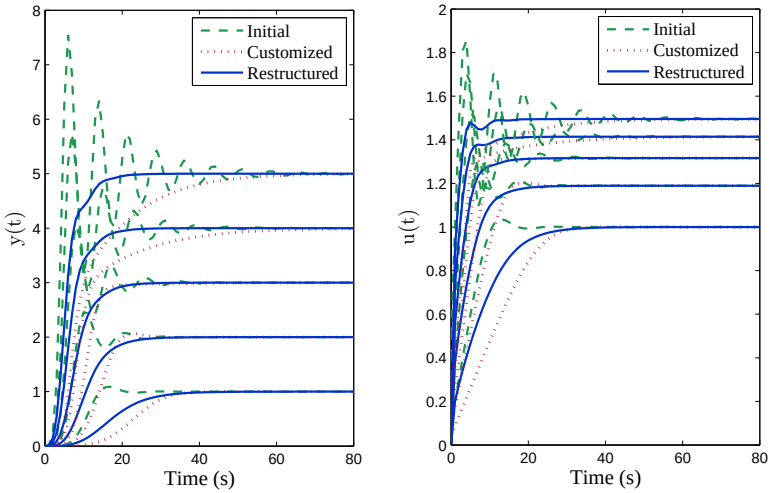

Figure 4.2. Step responses of the initial and restructured controllers and their control efforts from the first platform at different reference magnitudes as well as those of the customized controller in Fig. 3.1

ing. Supported by these results, the solutions shown henceforth are obtained with scaled $\mathbf{\Phi}_\gamma$.

Table 4.2. Range of condition numbers of the structural sensitivity matrix $\mathbf{\Phi}_\gamma$ and the lowest absolute output error sum found during controller restructuring of the first platform with and without scaling of $\mathbf{\Phi}_\gamma$ by δM_i from Eq. (2.10)

Reference Magnitude	Condition Number of Φ_γ unscaled	scaled	Lowest Error ($\min \sum_{i=1}^{N} \lvert\tilde{y}(t_i)\rvert$) unscaled	scaled
1	1.61 - 12.16	2.02 - 2.07	2.61	1.35
2	1.69 - 6.95	1.80 - 2.68	4.37	2.50
3	2.13 - 4.94	1.07 - 4.69	6.10	2.65
4	10.03 - 14.05	1.09 - 2.67	8.18	3.99
5	13.37 - 13.53	1.09 - 4.48	11.38	6.10

4.1.2 Controller for the Inverted Pendulum on a Cart

For the inverted pendulum on the cart, the candidate controllers were generated from the state feedback controller $K_1x + K_2\dot{x} + K_3\theta + K_4\dot{\theta}$ using $[f_1, f_2, f_3, f_4] = \left[|x|, |\dot{x}|, |\theta|, |\dot{\theta}|\right]$ in Eq. (2.5). To invoke the nonlinearity of the pendulum, an impulse

magnitude of $\delta = 18$ (see Fig. 3.5) was applied to the cart, using the closed-loop response of the linear controller to an impulse magnitude of $\delta = 15$ as the desired response. Each candidate controller was adapted for 15 iterations in the round robin phase and the best controller was adapted for 50 iterations in the final phase. The restructured controller had the form

$$u(t) = -K_1 x(t) - K_2 \dot{x}(t) - K_3 \theta(t) - K_4 \dot{\theta}(t) \implies u(t) = -K_1 x(t) \left|\dot{\theta}(t)\right|^{0.04} - K_2 \dot{x}(t) \left|\dot{\theta}(t)\right|^{0.02} - K_3 sgn(\theta(t)) \left|\theta(t)\right|^{0.92} - K_4 sgn(\dot{\theta}(t)) \left|\dot{\theta}(t)\right|^{1.03} \quad (4.2)$$

The responses and control efforts of the restructured and linear controllers at the impulse magnitude of $\delta = 18$ are shown in Fig. 4.3 along with the desired response. They indicate the more rapid response than its linear counterpart of the restructured controller in stabilizing the pendulum.

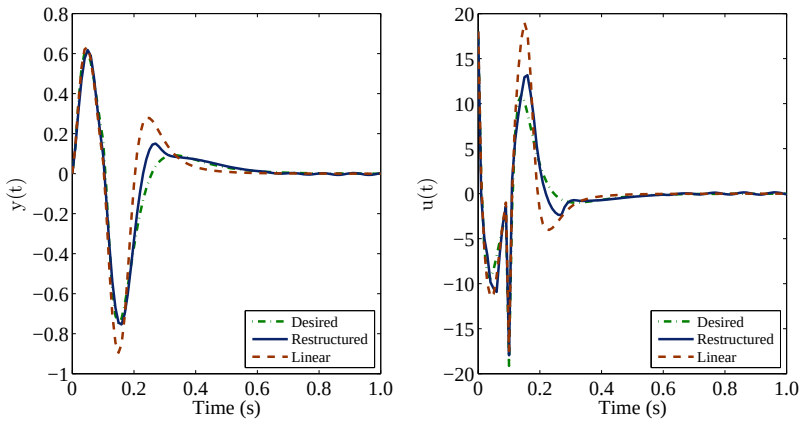

Figure 4.3. Impulse responses and control efforts of the linear and restructured controllers from the inverted pendulum on a cart (second platform) shown with the desired response used for controller restructuring

As benchmark, the impulse responses of the inverted pendulum on a cart with the restructured controller (Eq. (4.2)) are compared with those of the linear controller at different impulse magnitudes in Fig. 4.4. Both the responses and control efforts of the restructured controller are significantly more robust than those of the

linear controller at different impulse magnitudes. This robustness is due in part to the quicker response of the restructured controller to state changes in the system, providing the capacity to cope with impulses of higher magnitude, as discussed in the next section.

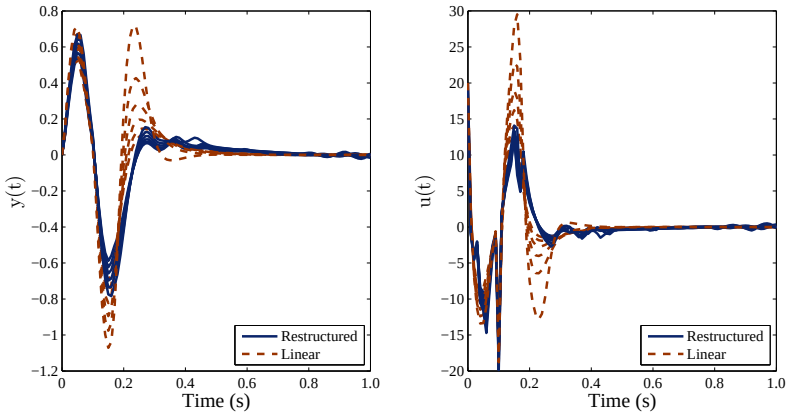

Figure 4.4. Impulse responses and control efforts of the linear and restructured controllers from the inverted pendulum on a cart at impulse magnitudes of 15-20

CHAPTER 5

ANALYSIS OF THE RESULTS & DISCUSSION

5.1 Analysis

The case study results obtained can be used to analyze several aspects of the restructured controllers by MSAM. One such aspect is the response of the restructured controllers to conditions absent in training, such as measurement noise, disturbances, and reference magnitudes beyond those used for training. A second aspect is the sensitivity of the restructured controllers to training conditions. A third aspect is the form and behavior of restructured components of the controllers in comparison to their initial counterparts.

5.1.1 Unrepresented Conditions

- *Noise:* To evaluate the performance of restructured controllers in presence of noise, band-limited noise at the signal-to-noise ratio of 18 (at $r = 1$) to 33 (at $r = 5$) was added to the output of the plant in the nonlinear actuator platform. Controller responses were tested ten times for different random noise cases, as shown in Fig. 5.1. The results indicate similarly affected closed-loop responses by measurement noise of both the restructured and customized controllers with smaller variations observed in the control efforts.

- *Disturbance rejection:* The disturbance rejection capacity of the controllers were evaluated in platform one with unit step disturbances applied before and after the plant $G_0(s)$ in Fig. 3.1. The closed-loop responses of both the restructured and customized controllers are shown in Fig. 5.2. The results

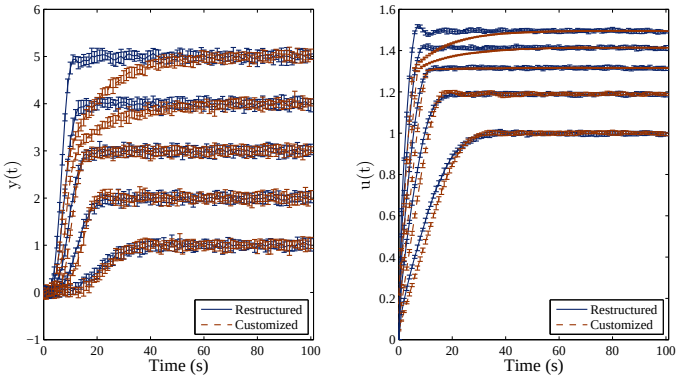

Figure 5.1. Closed-loop step response and control effort ranges of the first platform by restructured and customized controllers in presence of additive band-limited measurement noise at the approximate signal-to-noise ratios of 18 at $r = 1$ to 33 at $r = 5$

indicate much more agile disturbance rejection by the restructured controller at higher reference magnitudes, replicating the faster step response of these controllers at higher reference magnitudes in Fig. 4.2.

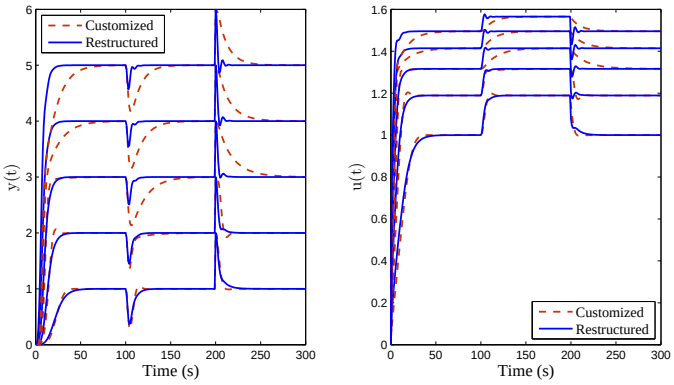

Figure 5.2. Closed-loop responses and control efforts of the first platform by restructured and customized controllers to unit step disturbances before $G_0(s)$ in Fig. 3.1 (at time 100) and after $G_0(s)$ (at time 200)

- *Different reference magnitude:* To evaluate the controllers' regulation capacity of the first platform for levels not encountered in training, the closed-loop step responses of the restructured controller are compared to those of the cus-

tomized controller at step sizes of 6-15 for the nonlinear actuator in Fig. 5.3. The results indicate that the restructured controller starts having oscillatory behavior at step sizes of 9 and higher, while the customized solution provides continually increasing sluggish response at these higher steps. Similarly, the closed-loop impulse responses of the inverted pendulum on a cart with the restructured and linear controllers were obtained at impulse magnitudes of 21-33. The linear controller was found to be deficient in maintaining upward position for the pendulum for impulse magnitudes of 27 and higher. The responses obtained with the restructured controller for impulse magnitudes of 27-33 are shown in Fig. 5.4. The results in Fig. 5.4 reveal the ability of the restructured controller in maintaining a stable response under conditions beyond the capacity of linear control.

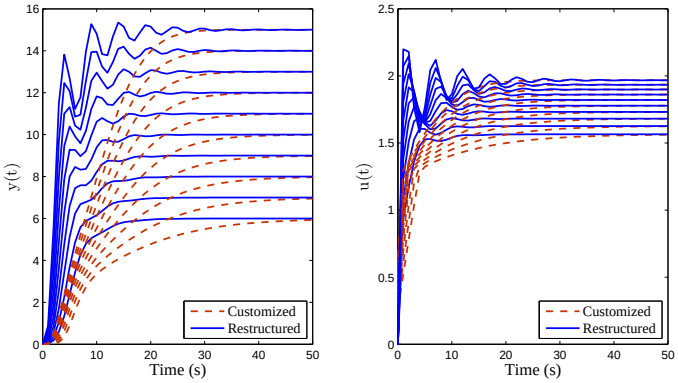

Figure 5.3. Closed-loop responses and control efforts of the first platform by restructured and customized controllers at higher step sizes (6-15) than those (1-5) used for restructuring

- *Modelling uncertainties:* To evaluate their robustness restructured controllers to modeling uncertainty, the closed-loop responses for the nonlinear actuator platform were generated first with the actuator nonlinearities of $f(u) = u^{3.5}$ and $f(u) = u^{4.5}$, as shown in Fig. 5.5. The responses of the restructured controller in Fig. 5.5 are quite similar, unlike those of the customized controller,

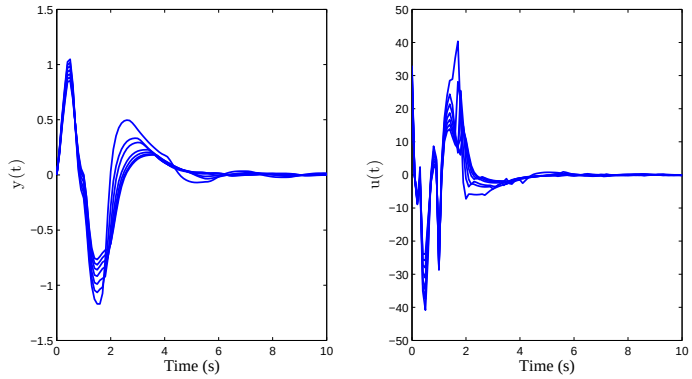

Figure 5.4. Closed-loop impulse responses and control efforts of the inverted pendulum on a cart (second platform) by the restructured controller (obtained at the impulse magnitude of 20) at impulse magnitudes of 27-33 that are beyond the capacity of the linear controller

even though the controller was restructured for the nominal actuator model of $f(u) = u^{4.0}$. The similarity of these responses indicates the robustness of the restructured controller to modeling uncertainty of actuator nonlinearity. Second, closed-loop responses of the inverted pendulum on a cart were obtained with 10%, 20%, and 30% smaller pendulum mass with the linear and restructured controllers, as shown in Fig. 5.6. The responses with the restructured controller in Fig. 5.6 are very close for different pendulum masses, particularly in comparison to those with the linear controller. They, like those for the nonlinear actuator, indicate the lower sensitivity of the restructured controllers to modeling uncertainty.

5.1.2 Sensitivity to Training Conditions

As was discussed earlier and depicted by the controller forms in Table 4.1, the training conditions influence the controller forms. For the first platform, sensitivity to training conditions was remedied by adopting a staircase format for restructuring the controllers for the nonlinear actuator. It, therefore, behooves us to examine the sensitivity of the controller forms to different staircase scenarios. Similarly, the

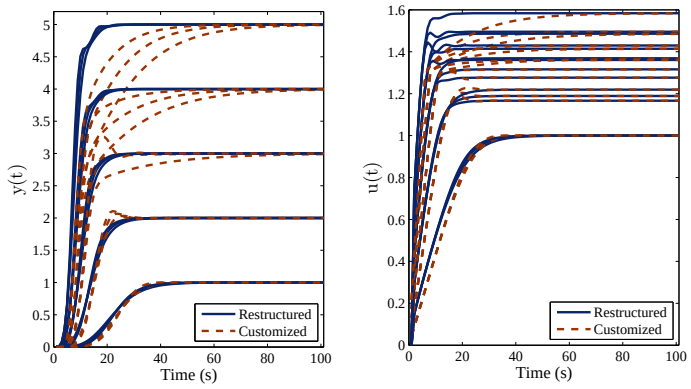

Figure 5.5. Step responses and control efforts of the first platform by restructured and customized controllers (Fig. 3.1) as affected by inaccurate actuator nonlinearities

restructured controller for the inverted pendulum on a cart was obtained at one impulse magnitude (δ = 18). So it raises the question as how the controller forms differ at different impulse magnitudes. To this end, the controller forms obtained for the nonlinear actuator and inverted pendulum from different training cases are shown in Table 5.1. The results indicate two controller forms found across the ten different staircase combinations (e.g., 1,2,3; 1,3,5; 2,3,4; etc.) for the nonlinear actuator and three controller forms for the inverted pendulum at three different impulse magnitudes. The difference between the controller forms for the nonlinear actuator is in the first component wherein the ϵ is coupled with itself, in the first case, and with its integral, in the second case. The restructured controller forms for the inverted pendulum on a cart, however, are quite diverse and can be compared better through their simulated behavior, as presented below.

5.1.3 Controller Components

The different forms obtained for the restructured controllers raise two important questions: (1) how different are the individual components of the controller from each other in different forms and from their counterparts in the initial con-

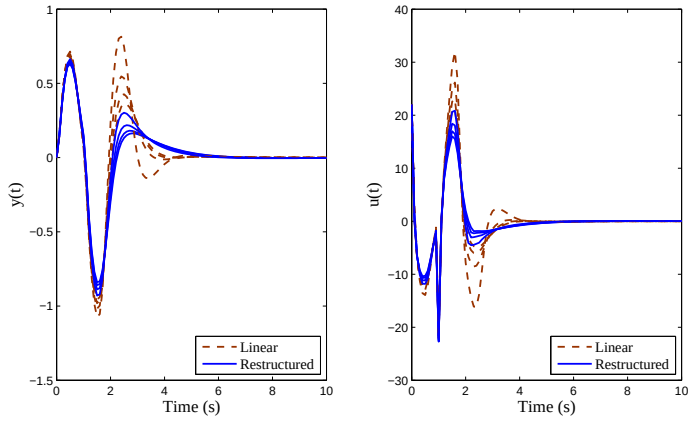

Figure 5.6. Closed-loop impulse responses and control efforts of the restructured and linear controllers for the inverted pendulum on a cart with inaccuracies of 0%, 10%, 20% and 30% in the pendulum mass

troller? and (2) how differently do they contribute to the total control effort? To address these questions, the numerical values of the individual components in Table 5.1 were obtained from simulation, as shown in Fig. 5.7 for the nonlinear actuator and in Fig. 5.8 for the inverted pendulum on a cart. The results in Fig. 5.7 indicate that the proportional effect "$K_p sgn\left(\epsilon(t)\right)\left|\epsilon(t)\right|^{(\gamma_1+1)}$" provides a smaller portion of the overall effort than "$K_p\epsilon(t)\left|\int \epsilon \mathrm{d}t\right)|^{\gamma_1}$", and that it has a nonzero initial value because of its entire dependence on the "$\epsilon(t)$". Its counterpart, however, is initially null due to its dependence on "$\int \epsilon \mathrm{d}t$" before it rises rapidly to its maximum value. The integral components, which have the same form, only differ slightly due to differences in the magnitude of "$\int \epsilon \mathrm{d}t$" in the two simulation runs.

The results in Fig. 5.8, however, show a much more nuanced difference of the controller components. They not only differ in form but also coefficient and exponent values. For instance, consider the similar in form "x effort" of the restructured controller at the impulse magnitudes of $\delta = 18$ and $\delta = 20$. Simulated in the first row of Fig. 5.8 (columns 1 and 3), despite their identical form their behavior is more different from those at $\delta = 18$ and $\delta = 19$ (columns 1 and 2), that are differ-

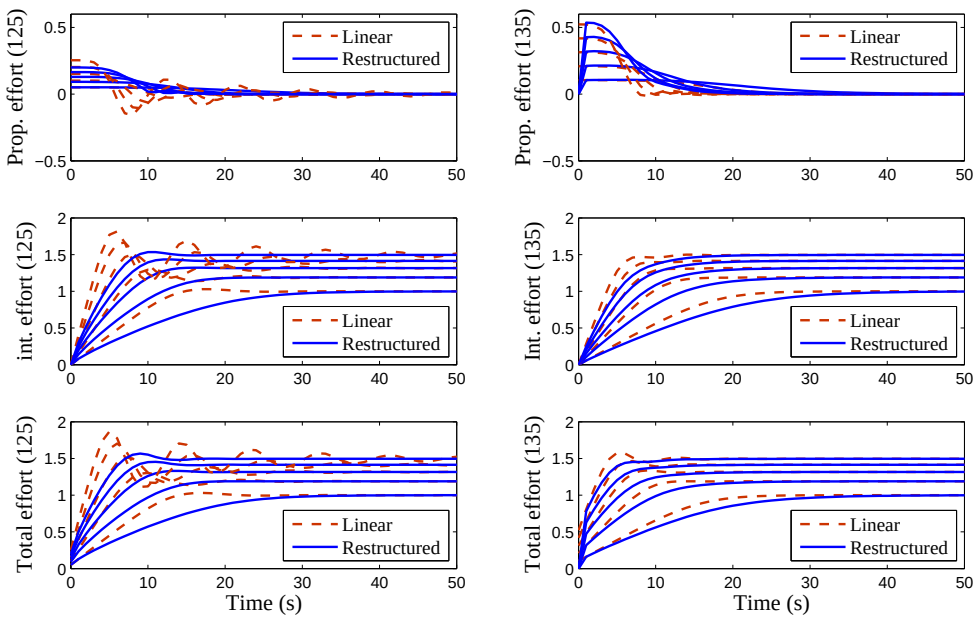

Figure 5.7. Components of the control efforts of the linear and restructured controllers with the two forms in Table 5.1 for the nonlinear actuator in response to step of magnitudes of 1-5

Table 5.1. Restructured controllers obtained from different staircase scenarios for the nonlinear actuator and at different impulse magnitudes for the inverted pendulum

	Restructured Controller
Step Sizes	**Nonlinear Actuator**
1,2,5	$K_p sgn\left(\epsilon(t)\right)\left\|\epsilon(t)\right\|^{(\gamma_1+1)} + K_i sgn(\int \epsilon \mathrm{d}t)\left\|\int \epsilon \mathrm{d}t\right\|^{(\gamma_2+1)}$
all others	$K_p \epsilon(t)\left\|\int \epsilon \mathrm{d}t\right)\|^{\gamma_1} + K_i sgn(\int \epsilon \mathrm{d}t)\left\|(\int \epsilon \mathrm{d}t)\right\|^{(\gamma_2+1)}$
Impulse Magnitude	**Inverted Pendulum on a Cart**
$\delta = 18$	$K_1 x(t)\left\|\dot{\theta}(t)\right\|^{\gamma_1} + K_2 \dot{x}(t)\left\|\dot{\theta}(t)\right\|^{\gamma_2} + K_3 sgn\theta(t)\|\theta(t)\|^{\gamma_3+1}$ $+K_4 sgn(\dot{\theta}(t))\left\|\dot{\theta}(t)\right\|^{\gamma_4+1}$
$\delta = 19$	$K_1 x(t)\left\|\theta(t)\right\|^{\gamma_1} + K_2 sgn(\dot{x}(t))\left\|\dot{x}(t)\right\|^{(\gamma_2+1)} + K_3 sgn(\theta(t))\left\|\theta(t)\right\|^{(\gamma_3+1)}$ $+K_4 \dot{\theta}(t)\left\|\dot{x}(t)\right\|^{\gamma_4}$
$\delta = 20$	$K_1 x(t)\left\|\dot{\theta}(t)\right\|^{\gamma_1} + K_2 \dot{x}(t)\left\|\theta(t)\right\|^{\gamma_2} + K_3 \theta(t)\left\|\dot{x}(t)\right\|^{\gamma_3}$ $+K_4 \dot{\theta}(t)\left\|\theta(t)\right\|^{\gamma_4}$

ent in form. This difference is presumed to be attributed to the confluence of the other components. Another observation of interest from Fig. 5.8 is the similarity between the total control efforts, shown in the last row of this figure, despite the very different behavior of individual components.

5.2 Discussion

- *Stability:* As with any controller design, of concern is the stability of the closed-loop systems with restructured controllers. Fortunately, a fundamental benefit of the proposed restructuring format, as schematized in Fig. 1.1, is its intrinsic evaluation of the candidate controllers in simulation. Since MSAM is designed to produce a controller that is at least better than the initial controller, it disregards any candidate controllers that are inferior in performance to other candidate controllers or the initial controller. Given that the instability of the system is a natural criterion in this performance

evaluation, the solutions delivered by MSAM are guaranteed to be closed-loop stable within the bounds of simulation incorporated in restructuring. Outside these bounds, analysis such as that presented in Section 5.1.1 can be used to identify instabilities unrepresented during restructuring. Analytical approaches to stability can also be used, though they are outside the breadth of present study.

- *Reachability:* In general, MSAM is additive by nature, designed to adapt a potentially inadequate initial controller by adding coupling to its individual components. Accordingly, this method is suited to restructuring initial controllers that are simple in form, as the restructured controllers are guaranteed to be more complex than their initial version. Furthermore, MSAM operates with the assumption that a potentially superior restructured controller is reachable by prescribed adjustments to the components of the initial controller. To this end, the selection of the adjustments $\hat{f}_i$ in Eq. (2.5) is of paramount importance.

- *Scalability:* The scalability of MSAM depends on the number of candidate controllers considered during the round robin phase. Given that with n adjustments applied to Q components, Q^n candidate controllers need to be examined during the round robin phase, the selection process can become overwhelming if the controllers are examined sequentially. Fortunately, the examination of individual candidate controllers is independent of the others, therefore, this phase can be run in parallel, reducing the computation time to Q^n/p, with p denoting the number of processors. For large-scale problems that cannot be exhaustively searched, one can choose a subset of round robin controllers that are mechanistically plausible.

- *Algorithmic issues:* As with any other gradient-based search routine, the search process may be sensitive to several parameters. One such parameter is the size of the perturbation $\delta\gamma_i$ in Eq. (2.10) used for computing the structural sensitivities. Another is the initial value of μ in Eq. (2.13) that is adjusted at each iteration step. A third parameter is the perturbation size of the individual parameters used for computing $\partial\hat{y}/\partial\mathbf{\Theta}$ in Eq. (2.10). Yet a fourth parameter is the fitness function used to evaluate the candidate models, currently formulated to consider the size of the error as well as the correlation of the candidate output with its target. Since the sensitivity of the search process to these parameters will depend upon the convexity of the error surface, they need to be evaluated in the context of each problem.

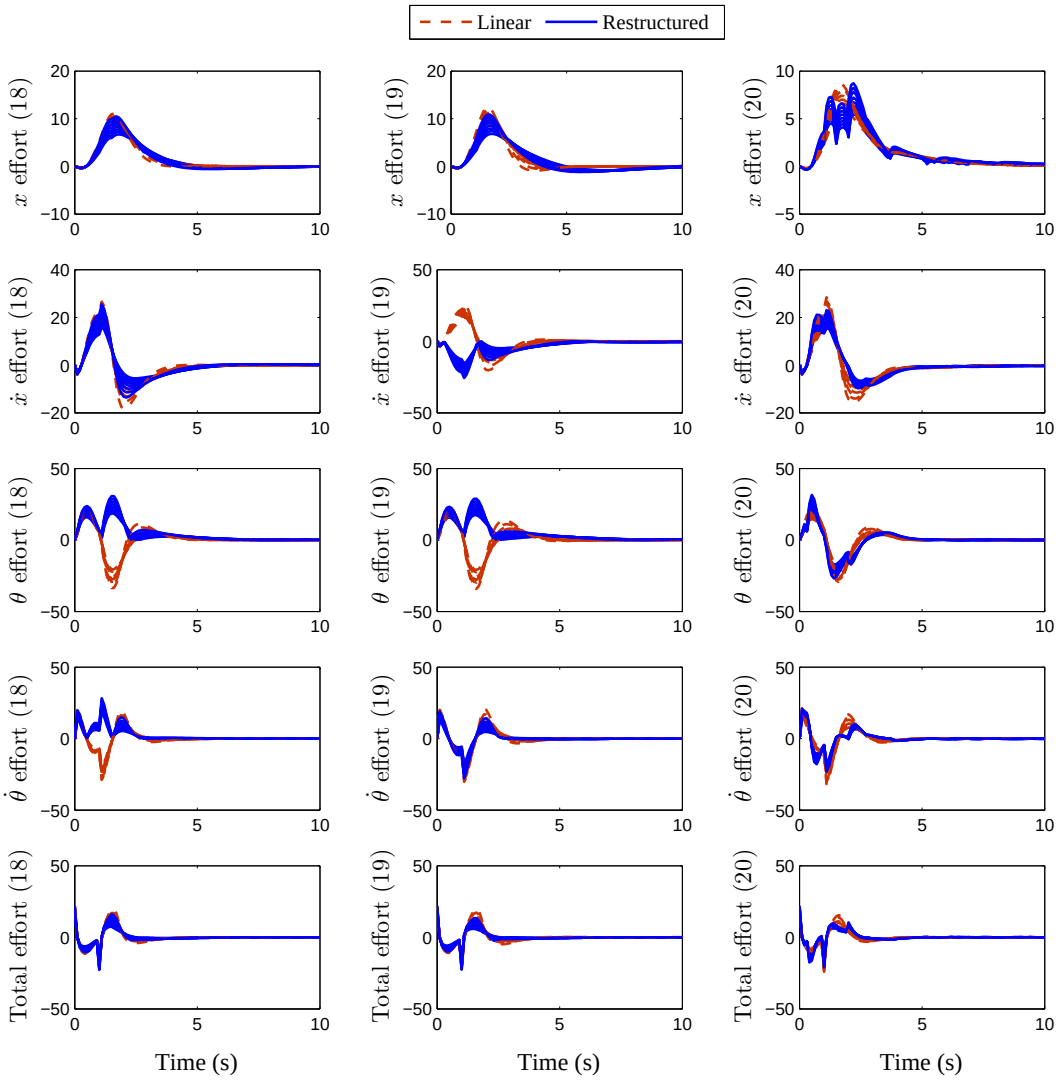

Figure 5.8. Components of the control efforts of the linear and restructured controllers with the three forms in Table 5.1 for the inverted pendulum in response to impulse magnitudes of 15-22

CHAPTER 6

CONCLUSION

A method for restructuring the controllers to accommodate nonlinearities in plants is been introduced that uses Model Structure Adaptation Method which is a gradient-based method of symbolic adaptation for continuous dynamic models. This method generates controllers that are intelligible in form, but more complex than an initial controller that is potentially inferior in performance. This method benefits from a metric for quantifying structural perturbations to controllers, which it uses to enable its reliable gradient-based adaptation of candidate controllers derived from the initial controller. The method is demonstrated in application to two benchmark problems, rendering solutions that are more effective in handling with plant nonlinearities and more robust to modeling uncertainties. The restructured controllers are also found to be more robust to conditions not introduced in training, including unseen reference magnitudes, noise and disturbances. In conclusion, the overall results obtained verify the original hypothesis of the work.

BIBLIOGRAPHY

[1] W. G. La Cava, K. Sahare, and K. Danai. Restructuring controllers to accommodate plant nonlinearities. *Journal of Dynamic Systems, Measurement, and Control*, 139(1):081004–081004–10, 2017.

[2] Karl J. Astrom and Bjorn Wittenmark. *Adaptive Control*. Dover Publications, Mineola, NY USA, second edition, 2008.

[3] William Messner and Dawn Tilbury. Control tutorials. `http://ctms.engin.umich.edu/CTMS/index.php?aux=Home`. Accessed: 2016-1-7.

[4] Gene F. Franklin, J. David Powell, Abbas Emami-NaeiniMiroslav Krstic, Ioannis Kanellakopoulos, and Petar Kokotovic. *Feedback Control of Dynamic Systems*. Pearson Education, Inc., Upper Saddle River, New Jersey, USA, seventh edition, 2015.

[5] Miroslav Krstic, Ioannis Kanellakopoulos, and Petar Kokotovic. *Nonlinear and Adaptive Control Design*. John Wiley and Sons, New York, NY, USA, 1995.

[6] R. Sepulchre, M. Jankovic, and P.V. Kokotovic. *Constructive Nonlinear Control*. Springer London, London, UK, 1997.

[7] Hassan K. Khalil. *Nonlinear Controls*. Pearson Education Inc, 1 Lake St., Upper Saddle River, NJ 07458, third edition, 2015.

[8] K. S. Narendra and A. M. Annaswamy. *Stable Adaptive Systems*. Prentice Hall, 1989.

[9] K. S. Narendra and K. Parthasarathy. Identification and control of dynamical systems using neural networks. *IEEE Trans. on Neural Networks*, 1(1):4–27, 1990.

[10] J. R. Koza. *Genetic Programming: On the Programming of Computers by Means of Natural Selection*. MIT Press, Cambridge, MA USA, 1992.

[11] P. J. Fleming and R. C. Purshouse. Evolutionary algorithms in control systems engineering: a survey. *Control Engineering Practice*, 10:1223–1241, 2002.

[12] Gilberto Reynoso-Meza, Xavier Blasco, Javier Sanchis, and MiguelMartnez. Controller tuning using evolutionary multi-objective optimisation: Current trends and applications. *Control Engineering Practice*, 28:58–73, 2014.

[13] S. A. Billings. *Nonlinear System Identification*. Wiley, 1st edition, 2013.

[14] W. G. La Cava and K. Danai. Gradient-based adaptation of continuous dynamic model structures. *International Journal of Systems Science*, 47(1):249–263, 2016.

[15] H. Hjalmarsson. Iterative feedback tuning - an overview. *Int'l J. of Adaptive Control and Signal Processing*, 16:373–395, 2002.

[16] Gevers M. Mossberg M. Bosmans E. Lequin, O. and L. Triest. Iterative feedback tuning of pid parameters: Comparison with classical tuning rules. *Control Engineering Practice*, 11(9):1023–1033, 2003.

[17] N. J. Killingsworth and M. Krstic. Pid tuning using extermum seeking. *IEEE Control Systems Magazine*, pages 70–79, Feb. 2006.

[18] J. R. McCusker, M. G. McKinley, and K. Danai. Iterative controller tuning in the time-scale domain. In *Proc. of 2009 Dynamic Systems and Control Conference*, Hollywood, California, October 2009. ASME.

[19] W. G. La Cava and K. Danai. Model structure adaptation: A gradient-based approach. In *Proceedings of DSCC 2015*, Columbus, Ohio, USA, Oct. 2015.

[20] M. Gevers. A decade of progress in iterative process control design - from theory to practice. *Journal of Process Control*, 12:519–531, 2002.

[21] J. E. Jackson. *A User's Guide to Principle Components*. John Wiley & Sons, Inc., 1991.